Dinosaur embryology: inside the bones of an Early Jurassic sauropodomorph from China

Robert R. Reisz[1*], Timothy D. Huang[2], Eric Roberts[3], ShinRung Peng[4], Corwin Sullivan[5], Koen Stein[6], Aaron LeBlanc[1], DarBin Shieh[4], RongSeng Chang[7], ChengCheng Chiang[8], ChuanWei Yang[9], ShiMing Zong[10]

[1]Department of Biology, University of Toronto Mississauga, Mississauga, ON L5L 1C6, Ontario, Canada. [2]National Chung Hsing University, Taichung 402, Taiwan. [3]School of Earth and Environmental Sciences, James Cook University, Townsville, Queensland, QLD 4811, Australia. [4]Medical College Institute of Oral Medicine, National Cheng Kung University, Tainan 701, Taiwan. [5]Key Laboratory of Evolutionary Systematics of Vertebrates, Institute of Vertebrate Paleontology and Paleoanthropology, 100044 Beijing, China.[6]Steinmann Institüt für Geologie, Mineralogie und Paläontologie, University of Bonn, 53115 Bonn, Germany. [7]Dept of Optics and Photonics, National Central University, Chung-Li, 32001, Taiwan. [8]National Synchrotron Radiation Research Center, Hsinchu 30076, Taiwan. [9]Lufeng County Dinosaur Museum, Lufeng, Yunnan, China. [10]ChuXiong Prefecture Museum, 675000 Chuxiong, Yunnan, China.

Fossil dinosaur embryos are surprisingly rare, almost entirely restricted to Upper Cretaceous strata that record the late stages of non-avian dinosaur evolution[1,2]. Notable exceptions are the oldest known embryos from the Early Jurassic South African sauropodomorph *Massospondylus*[3-4], and Late Jurassic embryos of a theropod from Portugal[5]. The fact that dinosaur embryos are rare and typically enclosed in eggshells limits their availability for tissue and cellular level investigations of development and growth. Consequently, little is known about growth patterns in dinosaur embryos, even though post-hatching ontogeny has been studied in several taxa[6]. Here we report the discovery of an embryonic dinosaur bonebed from the Lower Jurassic of China, the oldest such occurrence in the fossil record. The embryos are similar in geological age to those of *Massospondylus* and are also assignable to a sauropodomorph dinosaur, probably *Lufengosaurus*[7]. The unusual preservation of numerous disarticulated skeletal elements and eggshell in this monotaxic bone bed, representing different stages of incubation and therefore derived from different nests, provides opportunities for novel investigations of dinosaur embryology in a clade noted for gigantism. For example, comparisons among embryonic femora of different sizes and different developmental stages reveal a consistently rapid rate of growth throughout development, possibly indicating that short incubation times were characteristic of sauropodomorphs. In addition, asymmetric radial growth of the femoral shaft and rapid expansion of the fourth trochanter suggest that embryonic muscle activation played an important role in the pre-hatching ontogeny of these dinosaurs. This discovery also provides the oldest evidence of in situ preservation of complex organic remains in a terrestrial vertebrate.

Monotaxic bonebeds are particularly prized by palaeobiologists because they yield large numbers of bones that can reveal patterns of development and growth within a single species[8]. Here we report the discovery of a monotaxic embryonic dinosaur bonebed, from Lower Jurassic strata near Dawa, Lufeng County, Yunnan Province, People's Republic of China (specimens housed in the Chuxiong Prefectural Museum, Catalogue No. C2019 2A233). These remains are equivalent in age to the oldest known dinosaurian embryos, which belong to the South African sauropodomorph *Massospondylus*[3]. However, the new Chinese sauropodomorph specimens differ in comprising an accumulation of disarticulated skeletal elements representing various stages of embryonic development, rather than a set of articulated skeletons enclosed in eggs[9]. Thus, the earliest known dinosaurian embryo occurrences from China and South Africa are mutually complementary, permitting different types of investigation into the early stages of development in sauropodomorph dinosaurs that lived shortly after the end-Triassic extinction.

The embryonic bonebed was discovered in the Dark Red Beds or Zhangjia'ao Member[10, 11]of the Early Jurassic (Sinemurian, 190-197 Ma) Lower Lufeng Formation, roughly 3-5 m below the top of the formation (Fig. 1). The Lower Lufeng Formation is temporally, environmentally and faunally comparable to the Upper Elliot Formation of southern Africa and the Kayenta Formation of North America[12] (Supplementary Information 1). Like these similar rock units on other continents, the Lower Lufeng Formation preserves abundant skeletal remains of basal sauropodomorphs[13], and these dinosaurs are commonly found in the upper part of the Dark Red Beds[14].

Taphonomically, the 10-20 cm thick embryonic bonebed is characterized by the presence of completely disarticulated skeletal elements at various stages of embryonic development (Fig. 2), with calcium carbonate nodules often surrounding tightly packed appendicular skeletal elements. One nodule contains a high concentration of eggshell fragments that were apparently derived from soil compaction of a single egg. The latter material provides for the first time microstructural information about the oldest known terrestrial vertebrate eggshell (Supplementary Information 2, Supplementary Figs. 2.1-2.5).

We interpret the bonebed as a para-autochthonous assemblage, formed by low-energy flooding and slow inundation of a colonial nesting site. The host sediment is a heavily bioturbated, massive siltstone, throughout which are dispersed isolated skeletal elements, eggshell fragments and the small, fossil rich nodules of calcium carbonate. As a result, there are no preserved nest structures or uncrushed eggs. The lack of coarse-grained sediment, coupled with the apparent sorting and concentration of the bones (Fig. 2c, f, g), is intriguing from a taphonomic perspective. The bonebed does not appear to be an in situ nest or catastrophic death assemblage, but is also not a time-averaged fluvial deposit containing bones that were transported from beyond the immediate vicinity. The latter possibility is incompatible with the high preservational quality of the delicate, poorly ossified embryonic bones and <100 μm-thick eggshell, which would be expected to suffer extensive damage during transport over substantial distances. However, the presence of bones at different levels of development (i.e., from multiple clutches), coupled with the concentration and partial alignment of eggshell fragments and certain skeletal elements within the nodules (Fig. 2f), does indicate a degree of transport. We believe that inundation, ponding, and partial decomposition, followed by weak currents

and simple wave action, represents the best explanation for the hydrodynamic sorting and non-random orientation of the mostly disarticulated embryonic elements. The embryonic bones and egg shells were eventually buried and subjected to pedogenic processes, including bioturbation, soil compaction and expansion, and precipitation of carbonate nodules around many of the bones.

The skeletal remains, more than 200 bones, include dozens of isolated cervical, dorsal, and caudal centra, rib fragments, femora and other limb elements, scapulae, an ilium, and a few skull elements (Fig. 2). These specimens are less ontogenetically advanced in multiple respects than some previously known sauropodomorph, theropod and ornithischian skeletons that can be definitively identified as embryonic because they were discovered inside intact eggs, demonstrating that these specimens are embryos rather than hatchlings[15]. Conspicuously embryonic features include the presence of teeth that do not protrude beyond the alveolar edges of the maxilla and dentary, centra with large notochordal canals and deeply pitted articular surfaces, and the universal presence of extensive primary vascular spaces that are open to the surface[16-18] (Supplementary Information 3, Supplementary Fig. 3).

The embryonic bones were compared with previously known saurischian and ornithischian embryos, and found to share detailed resemblances with other sauropodomorph embryos but not with embryos of ornithischians or theropods[1-3]. In particular, identification of the Lufeng specimens as sauropodomorphan was greatly facilitated by their similarity to the well known, articulated *Massospondylus* embryos[19]. Interpretation of the embryonic bones as representing a basal sauropodomorph is based not only on numerous features that are synapomorphies at various levels within basal Sauropodomorpha, but also on the results of a phylogenetic analysis using data from a recent study[20]. This analysis places the specimens well within the sauropodomorph clade but well outside Sauropoda, and supports their tentative referral to the well-known Lufeng Formation sauropodormorph *Lufengosaurus*. Within Sauropodomorpha, the maxilla and its dentition show specific morphological resemblances to *Lufengosaurus*. This identification is also supported by the presence of a possible femoral autapomorphy (strong medial curvature of the distal part of the 4th trochanter) in the 24 embryonic femora and in the holotype of *L. huenei*[7]. However, two other basal sauropodomorphs have also been recovered from the Lower Lufeng Formation of Yunnan[14], making referral of the embryonic specimens to *Lufengosaurus* inescapably tentative. (Supplementary Information 4 and Supplementary Figs. 4.1, 4.2).

Histological study of the Lufeng embryonic specimens provides an unprecedented window into the process of embryonic growth in a dinosaur, because these fossils represent numerous individuals at various stages of embryonic development. For example, three thin-sectioned dorsal vertebrae show different stages in the embryonic development of the notochordal canal[17] (Fig. 3), a feature that is absent in posthatchlings. Longitudinal sections of two vertebrae (Fig. 3a, b) show that the cranial and caudal ends consist mostly of hypertrophied calcified cartilage. The mid-regions of the vertebrae show an initial stage of highly cancellous bone deposition, with numerous primary cavities ("vascular spaces"), indicative of very fast growth[21], and there is no evidence of any bone remodeling. A transverse section through the third vertebra (Fig. 3c) shows the notochordal canal as a large tunnel through the middle of the centrum, and reveals

erosion cavities that indicate resorption of the cartilaginous precursor. Small patches of calcified cartilage are still visible.

The sample includes 24 femora, including 14 right femora (MNI=14). The femora range from 2.6 to 4.5 mm in mid-shaft diameter and 12 to 22 mm in length, representing individuals from multiple nests[19], and permitting the first morphometric analysis of embryonic growth and development in a dinosaur (Fig. 4a, Supplementary Information 5, Supplementary Figs 5.1-5.4). Separate thin sections through the mid-shaft regions and 4th trochanters of three femora of different diameters also illustrate the development and ossification of the femur (Fig.4a-c). The cross sections show major differences in periosteal bone distribution, orientation of the vascular spaces (primary cavities), and size and level of ossification of the 4th trochanter (insertion site of the primary propulsive muscle of hindlimb). For example, in the smallest, least ossified femur (Fig. 4b), the 4th trochanter is small, in the mid-sized femur (Fig. 4c) the trochanter is more prominent, but this femur shows little woven bone tissue in the trochanter, while in the largest femur (Fig. 4d), the 4thtrochanter is large and fully ossified. These successive stages of embryological development have not been previously documented in dinosaurian embryos. Mid-shaft cross sections of seven femora, including the three listed above (Fig. 4b-d) show a significantly greater degree of vascularity (ratio of primary cavity area to total cross-sectional area of the cortex ranging from 56% to 65%) than in other dinosaurs, indicating a sustained very rapid rate of growth[21]. In addition, the femoral medullary cavity increases in diameter throughout embryonic development (Supplementary Fig. 5.4), indicating that, although the embryonic femur is composed entirely of primary bone, reshaping by endosteal bone resorption in the medullary cavity occurs even at this early stage of ontogeny. The high level of vascularity is the first known evidence that sauropodomorph embryos probably grew at a faster rate than both extant birds and other dinosaurs, a circumstance that may imply that sauropodomorphs had shorter incubation times than their contemporaries. If this high rate of growth was maintained after hatching, it might explain the ability of sauropodomorphs to consistently achieve larger adult size than their dinosaurian contemporaries, and in some taxa reach gigantic proportions.

Extant vertebrates can display considerable limb and body movement prior to birth or hatching, involving muscle activation that mediates skeletal development[22, 23]. In mice and chickens this epigenetic phenomenon results in differential (asymmetrical) thickening of the walls of the long bones for improved load-bearing, resulting in a condition similar to that in the embryonic sauropodomorph femora. Similarly, sustained growth of skeletal crests and flanges depends on activation of the muscles attached to them, an observation that should be applicable to the dinosaurian 4th trochanter. It is likely that the uneven thickening of the femoral walls in the Lufeng specimens, the circumferential orientation of the primary vascular cavities, and the growth of the 4thtrochanter (Fig. 4b-d) all depended upon muscle contraction and embryonic motility, an important mechanism for building a skeleton capable of coping with the functional demands encountered by the neonate. This discovery adds the first fossil evidence of such epigenetic phenomena to a growing body of research that documents their significance in extant model organisms.

The available isolated embryonic bones were also subjected to detailed analysis using Synchrotron Radiation Fourier Transformation Infrared (SR-FTIR) spectroscopy[25]. In contrast to previous studies that reported organic residues based on extracts obtained by decalcifying samples of bone, our analyses (Fig. 5) were able to target particular

tissues in situ. Our approach made it possible to detect the preservation of organic residues, likely direct products of the decay of complex proteins, within both the fast growing embryonic bone tissue and the margins of the vascular spaces (Fig. 5a, b). This is indicated by the multiple amide peaks revealed by both infrared (1,500-1,700 cm^{-1} strong band from amide I & II, and 1,200-1,300 cm^{-1} weak band from amide III) and Raman spectroscopy (Amide A peak at 3,264 cm^{-1}) (Supplementary Figs 6.1, 6.2). Previous reports of dinosaur organic remains, or "dinosaurian soft tissues"[26-28], have been controversial because it was difficult to rule out bacterial biofilms or some other form of contamination as a possible source of the organics[29, 30]. Our results clearly indicate the presence of both apatite and amide peaks within the woven embryonic bone tissue (Fig. 5a), which should not be susceptible to microbial contamination or other postmortem artefacts. Future work on the embryonic specimens will include more detailed analysis of the nature of the organic remains that we have detected in these bones. However, their preservation in such delicate, porous structures raises the very real possibility that other fossils may also contain native soft tissues that can be studied with this targeted approach, opening up new areas of palaeobiological research.

Methods Summary

Fossil preparation was done manually under a dissecting microscope. Thin sections ranging from 30 to 50 μm in thickness were produced with minimal loss of tissue, and photographed using a Nikon AZ100 microscope with a lambda filter. ImageJ software was used to calculate the percentage vascularity of each femoral thin section, defined as the ratio between the total area of the primary cavities and the overall area of the cortex of the femur. NIS Elements imaging software for the Nikon AZ100 mounted digital camera was used both for the photography and to confirm the percentage vascularity calculations for a total of 8 femora. For FTIR analysis, infrared spectral line scans and mapping data were collected using the SR-FTIR spectromicroscopy facility at the National Synchrotron Radiation Research Center (NSRRC) beamline 14A1 (BL14A1) in Taiwan. The spectra were recorded in reflectance mode from each sample section, using a Thermo Nicolet Magna-IR spectrometer with the following settings: resolution 4 cm^{-1}, step-size 15 μm, aperture size 30 μm, and 128 scans. Peak position and baseline corrections were performed using OMNIC peak resolving software after the results had been obtained.

1. Carpenter, K., Hirsch, K., & Horner J. R. eds. *Dinosaur Eggs and Babies*. 372 pp. (Cambridge Univ. Press, Cambridge, 1994).
2. Chiappe, L. M. et al. Sauropod dinosaur embryos from the Late Cretaceous of Patagonia. *Nature* **396**, 258-261 (1998).
3. Reisz, R. R., Scott, D., Sues, H.-D., Evans, D. C. & Raath, M. A.. Embryos of an Early Jurassic prosauropod dinosaur and their evolutionary significance. *Science* **309**, 761-764 (2005).
4. Reisz, R. R., Evans, D. C., Roberts, E. M., Sues, H.-D., & Yates, A. M. Oldest known dinosaurian nesting site and reproductive biology of the Early Jurassic sauropodomorph *Massospondylus*. *Proc.Natl.Acad.Sci. USA* **109**, 2426-2433 (2012).
5. Ricqlès, A. D., Mateus, O., Antunes, M. T. & Taquet, P. 2001. Histomorphogenesis of embryos of Upper Jurassic theropods from Lourinhã (Portugal). *C. R. l'Acad. Sci.,*

Paris, Earth and Planetary Sci. **332**, 647-656 (2001).
6. Padian, K., de Ricqles, A. J. & Horner, J. R. Dinosaurian growth rates and bird origins. *Nature,* **412,** 405-408 (2001).
7. Young, C. C. A complete osteology of *Lufengosaurus huenei* Young (gen. et sp. nov) from Lufeng, Yunnan, China. *Palaeontol. Sinica, N S C* 7:1–53 (1941).
8. Rogers, R. R., Eberth, D. A. & Fiorillo, A. R. eds. *Bonebeds, Genesis, Analysis, and Paleobiological Significance.* Chicago Univ. Press, Chicago, 2007)
9. Carpenter, K. *Eggs, nests, and baby dinosaurs. A look at dinosaur reproduction*. (Indiana Univ. Press, Bloomington, 1999).
10. Bien, M. N. "Red Beds" of Yunnan. *Bull. Geol. Soc. China* **21**, 159–198 (1941).
11. Fang, X. et a. in *Proceedings of the Third National Stratigraphical Congress of China.* 208–214 (Geological Publishing House, Beijing, 2000).
12. Weishampel, D. B., Dodson, P., and Osmólska, H. (eds.). 2004. *The Dinosauria.* (Univ. California Press, Berkeley, 2004).
13. Sun, A. G. & Cui, K. H. in *The Beginning of the Age of Dinosaurs.* (ed. Padian, K.) 275-278 (Cambridge Univ. Press, New York, 1986).
14. Galton, P. M. & Upchurch, P. in *The Dinosauria* (eds. Weishampel D. B., Dodson, P. & Osmolka, H.) 232-258 (Univ. California Press, Berkeley, 2004).
15. Kundrát, M., Cruickshank, A.R.I., Manning, T.W. & Nudds, J. Embryos of therizinosauroid theropods from the Upper Cretaceous of China: diagnosis and analysis of ossification patterns. *Acta Zoologica* (Stockholm) 89: 231–251. (2008).
16. Goodrich, E. S. *Studies on the Structure and Development of Vertebrates*. (Univ. Chicago Press, Chicago, 1930).
17. Fleming, A., Keynes, R. J., &Tannahill, D. The role of the notochord in vertebral column formation. *J. Anat.* **199**, 177–180 (2001).
18. Francillon-Vieillot, H.,et al. in Skeletal biomineralization: Patterns, processes and evolutionary trends. (ed. Carter, J. G) 471-530 (Van Nostrand Reinhold, New York, 1990).
19. Reisz, R. R., Sues, HD., Evans**,** D. C. & Scott, D. Embryonic skeletal anatomy of the Early Jurassic prosauropod dinosaur *Massospondylus*. *J. Vertebr. Paleontol.* **30,** 1653-1665 (2010).
20. Apaldetti, C., Pol, D., &Yates A. The postcranial anatomy of *Coloradisaurus brevis* (Dinosauria: Suropodomorpha) from the Late Triassic of Argentina and its phylogenetic implications. *Palaeontology* DOI: 10.1111/j.1475-4983.2012.01109.x (2012).
21. Horner, J. R., Padian, K. & Ricqlès, A. D. Comparative osteohistology of some embryonic and neonatal archosaurs: implications for variable life histories among dinosaurs. *Paleobiology* **27**, 39-58. (2001).
22. Müller, G. B. Embryonic motility: environmental influences and evolutionary innovation. *Evolution & Development* **5**, 56-60 (2003).
23. Sharir, A., Stern, T., Rot, C., Shahar, R. & Zelzer, E. Muscle force regulates bone shaping for optimal load-bearing capacity during embryogenesis. *Development* **138**, 3247-3259 (2011).
24. Blitz, E. et al. Bone ridge patterning during musculoskeletal assembly is mediated through SCX regulation of *Bmp4* at the tendon-skeleton junction. *Developmental Cell* **17**: 861-873 (2009).

25. Kong J. & Shaoning, Y. Fourier Transform Infrared Spectroscopic Analysis of Protein Secondary Structures, *Acta Biochimica et Biophysica Sinica* **39(8),** 549-559 (2007).
26. Schweitzer, M. H., Wittmeyer, J. L., Horner, R. H. & Toporski J. K. Soft-Tissue Vessels and Cellular Preservation in *Tyrannosaurus rex*. *Science* **307**,1952-1955 (2005).
27. Schweitzer, M. H. et al. Analyses of soft tissue from *Tyrannosaurus rex* suggest the presence of protein. *Science* **316**, 277-280 (2007).
28. Lindgren J. et al. Microspectroscopic Evidence of Cretaceous Bone Proteins. *PLoS One* **6**, e19445 (2011).
29. Peterson, J. E., Lenczewski, M. E. & Scherer R. P. Influence of Microbial Biofilms on the Preservation of Primary Soft Tissue in Fossil and Extant Archosaurs. *PLoS One* **5**, e13334 (2010).
30. Kaye, T. G., Gaugler, G. & Sawlowicz, Z. Dinosaurian soft tissue interpreted as bacterial biofilms. *PloS One* **3(7),** e2808 (2008).

Supplementary Information is linked to the online version of the paper at www.nature.com/nature.

Acknowledgements We thank G. Grellet-Tinner, J. Steigler, P. Barrett, and E. Prondvai for discussion, C. Chu and X.J. Lin for research support, S.P. Modesto and C. Brown for field assistance, D. Scott for specimen preparation and photography, N. Campione for morphometric analysis, C. Apaldetti for data matrix, J.R. Liu for assistance in Lufeng, and C.C. Wang, Y.F. Song, Y.C. Lee, and H.S. Sheu for help with various experiments at the National Synchrotron Radiation Research Center, Taiwan. Research support was provided by DFG FOR 533 (Germany), NSC 100-2116-M-008-016 (Taiwan), Ministry of Education (Taiwan) under the NCKU Aim for the Top University Project, NSERC Discovery and SRO Grants (Canada), University of Toronto, Chinese Academy of Sciences and National Natural Science Foundation of China.

Author Contributions R.R.R jointly conceived and designed the project with T.D.H.; R.R.R. wrote paper, supervised preparation and scientific illustration of specimens; T.D.H., E.R., C.S., K.S., A.L., contributed to manuscript; R.R.R., T.D.H., E.R., C.S., R.S.C, and C.W.Y. contributed significantly to field work; T.D.H., S.R.P., D.B.S. supervised and completed multimodal optical and chemical spectroscopic analyses; K.S., A.L., C.C.C. prepared slides and illustrated thin sections; R.R.R., T.D.H., K.S., E.R., S.R.P., C.S. wrote Supplementary Information; T.D.H., R.S.C., C.W.Y., S.M.Z. provided logistical support for field work and research.

FIGURE CAPTIONS:

Figure 1. Location and stratigraphy of Lufeng monotaxic embryonic bone bed. **a**, Map of China, with study area in Yunnan Province shown by inset box. **b**, General

geological map of study area. **c**, Stratigraphic section showing location of embryonic bone bed within Zhangjia'ao Member of Lower Lufeng Formation.

Figure 2. **Sauropodomorph dinosaur embryonic skeletal elements derived from the Lufeng bone bed. a,** Reconstructed embryonic skeleton of Early Jurassic sauropodomorph (using *Massospondylus* as a model, not to scale), showing in dark red the elements known from Dawa **(**Chuxiong Prefectural Museum, Specimen No. C2019 2A233). Numerous ribs, centra, and distal limb elements are known, but their exact locations within the skeleton are difficult to determine. **b,** Left maxillae in ventromedial and labial views, respectively, with enlarged view of partially erupted tooth. **c,** mid-dorsal centrum in lateral and anterior views. **d,** Left ilium in lateral view. **e,** Right scapula, vertebrae, and left humerus preserved in one nodule. **f,** Right femur in posterolateral and medial views, showing prominence and shape of 4^{th} trochanter. **g,** Large right femur preserved with ribs and various other skeletal elements in nodule. **h,** Embryonic limb elements and ribs showing alignment along long axes. **i,** Close-up of proximal end of right tibia, showing external foramina of primary cavities (also called vascular canals). Scale bar = 1cm, unless otherwise shown.

Figure 3. Embryonic vertebral histology (C2019 2A233). a, Largest dorsal centrum, longitudinal section, cranial portion showing initial closure of notochordal canal (cd), and presence of erosion cavities (ee) with endochondral bone in the calcified cartilage (cc). A collar of periosteal bone (pb) has already been formed. **b**, Smallest dorsal centrum, longitudinal section showing whole length of bone, and representing earlier embryonic stage with widely open notochordal canal. **c**, Intermediate-sized dorsal centrum, transverse section, showing notochordal canal in cross section within substance of vertebral centrum (vc). Neural canal (nc) visible directly above notochordal canal. All scale bars equal 500 μm. Photographs taken with cross polar light with lambda filter.

Figure 4. Embryonic femoral morphometric analysis and histology (C2019 2A233). a, Results of regression analysis showing growth trajectory of femoral mid-shaft diameter relative to length of femur on left, and box-plot of residuals on right. Black dots represent Lufeng bonebed embryonic femora, blue dots represent two embryonic and one hatchling femora of the basal sauropodomorph *Massospondylus,* and red dot represents a hatchling femur of the sauropodomorph *Mussaurus.* The regression analysis is based solely on the Lufeng bonebed femora and shows a strong correlation between femoral length and shaft diameter, and there are no outliers in this sample. However, all specimens of the other two sauropodomorphs are well outside the range of variation exhibited by the Lufeng material, and exhibit thinner femora relative to their respective lengths. This is likely related to their presumed smaller egg, and eventual smaller and more gracile adult size (see Supplemental Information 5 and Supplemental. Figs 5.1-5.4 for data and additional morphometric analyses). **b-d,** Smallest to largest femora, sectioned transversely at mid-diaphysis and level of 4^{th} trochanter, from left to right. Photographs taken with cross polar light with lambda filter**.** Abbreviations: m, medullary cavity; tr, 4^{th} trochanter; nf, nutrient foramen; pb, primary periosteal bone with primary cavities ("vascular canals").

Figure 5. Synchrotron Radiation Fourier Transformed Infrared Spectroscopic (SR-

FTIR) analysis of embryonic femur, targeting different points within a small area of the bone (a-c). Images in each row include, from left to right: mosaic composed of 12 individual optical IR images (150x180 μm each), showing total FTIR scanned area (red box), specific point targeted for analysis (red cross) and 15 μm step size (red dots); 2D and 3D FTIR distributions of absorption for the spectral band showing the highest intensity at the targeted point, with blue and red corresponding to low and high absorption, respectively; and K-K correction processed IR spectrum for targeted point. **a,** FTIR scan targeting primary bone tissue, showing an apatite peak within the primary bone but not within the vascular spaces; primary bone tissue also shows an amide peak at 1,500-1,700 cm^{-1}, within the apatite crystal. **b,** FTIR scan targeting edge of vascular space, near primary bone tissue, showing that the margins of the vascular spaces are characterized by a 1,537 cm^{-1} amide I & II peak but lack an apatite peak. **c,** FTIR scan targeting central area of a vascular canal, showing an 885 cm^{-1} carbonate peak within the vascular spaces; a modest amide peak at 1,537 cm^{-1} is also present, and we interpret the carbonate peak as the result of calcite infilling of the vascular canals.

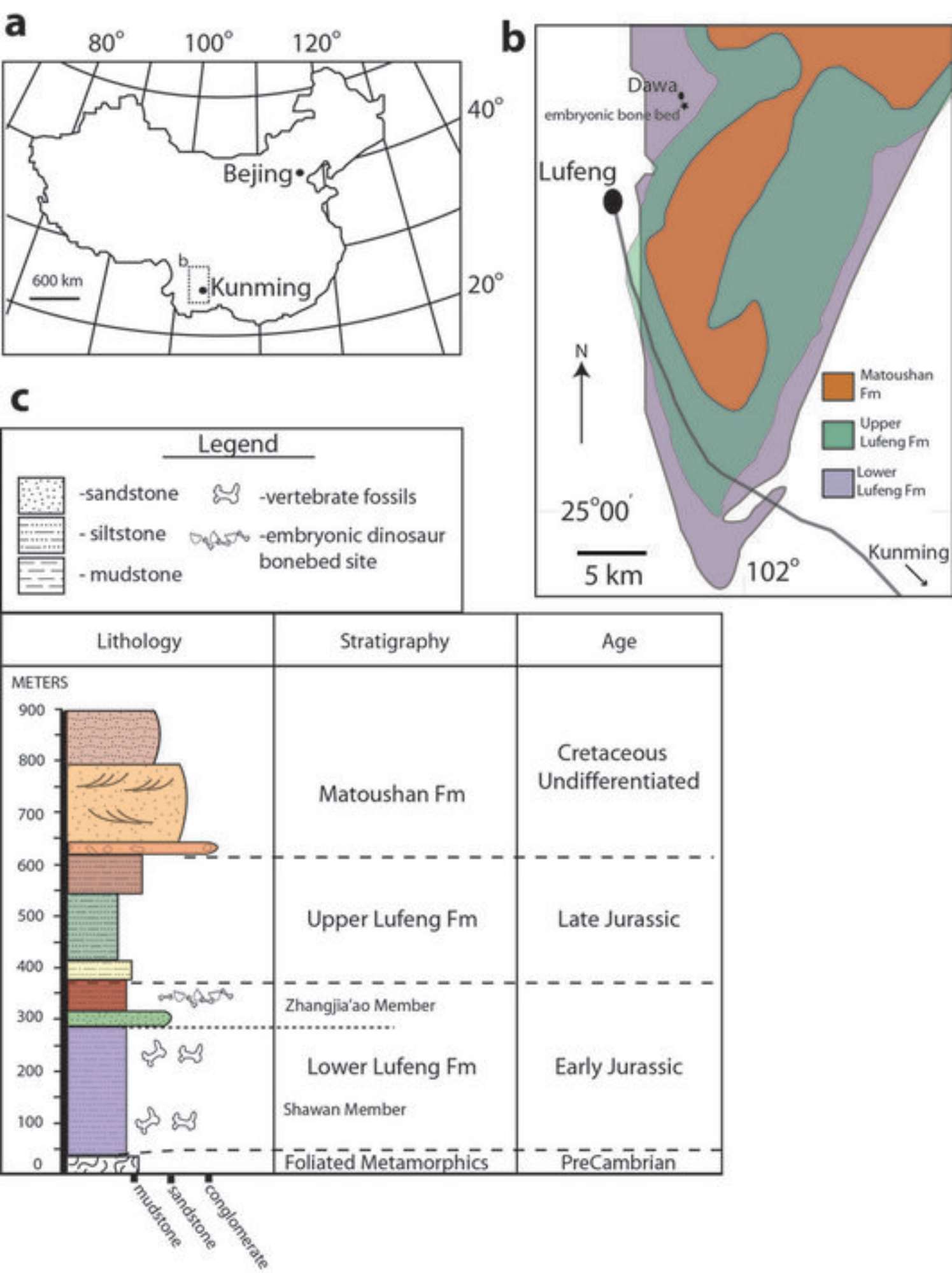
a
80°
100°
120°
40°
20°
Bejing
b
Kunming
600 km
b
Dawa
embryonic bone bed
Lufeng
N
Matoushan Fm
Upper Lufeng Fm
Lower Lufeng Fm
25°00′
5 km
102°
Kunming
c
Legend
-sandstone
- siltstone
- mudstone
-vertebrate fossils
-embryonic dinosaur bonebed site
Lithology
Stratigraphy
Age
METERS
900
800
700
600
500
400
300
200
100
0
Matoushan Fm
Cretaceous Undifferentiated
Upper Lufeng Fm
Late Jurassic
Zhangjia'ao Member
Lower Lufeng Fm
Early Jurassic
Shawan Member
Foliated Metamorphics
PreCambrian
mudstone
sandstone
conglomerate

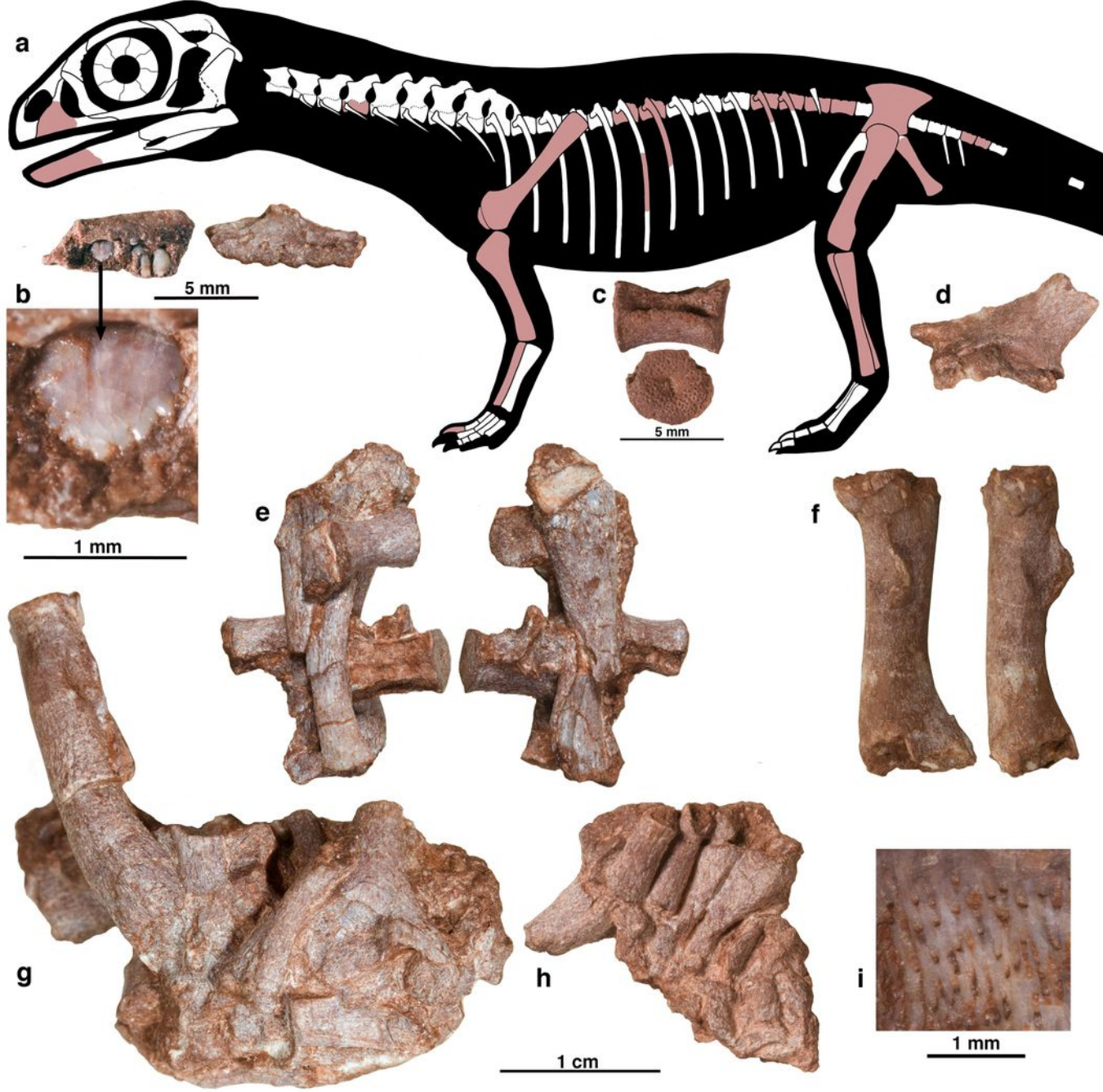
a
5 mm
b
1 mm
c
5 mm
d
e
f
g
h
1 cm
i
1 mm

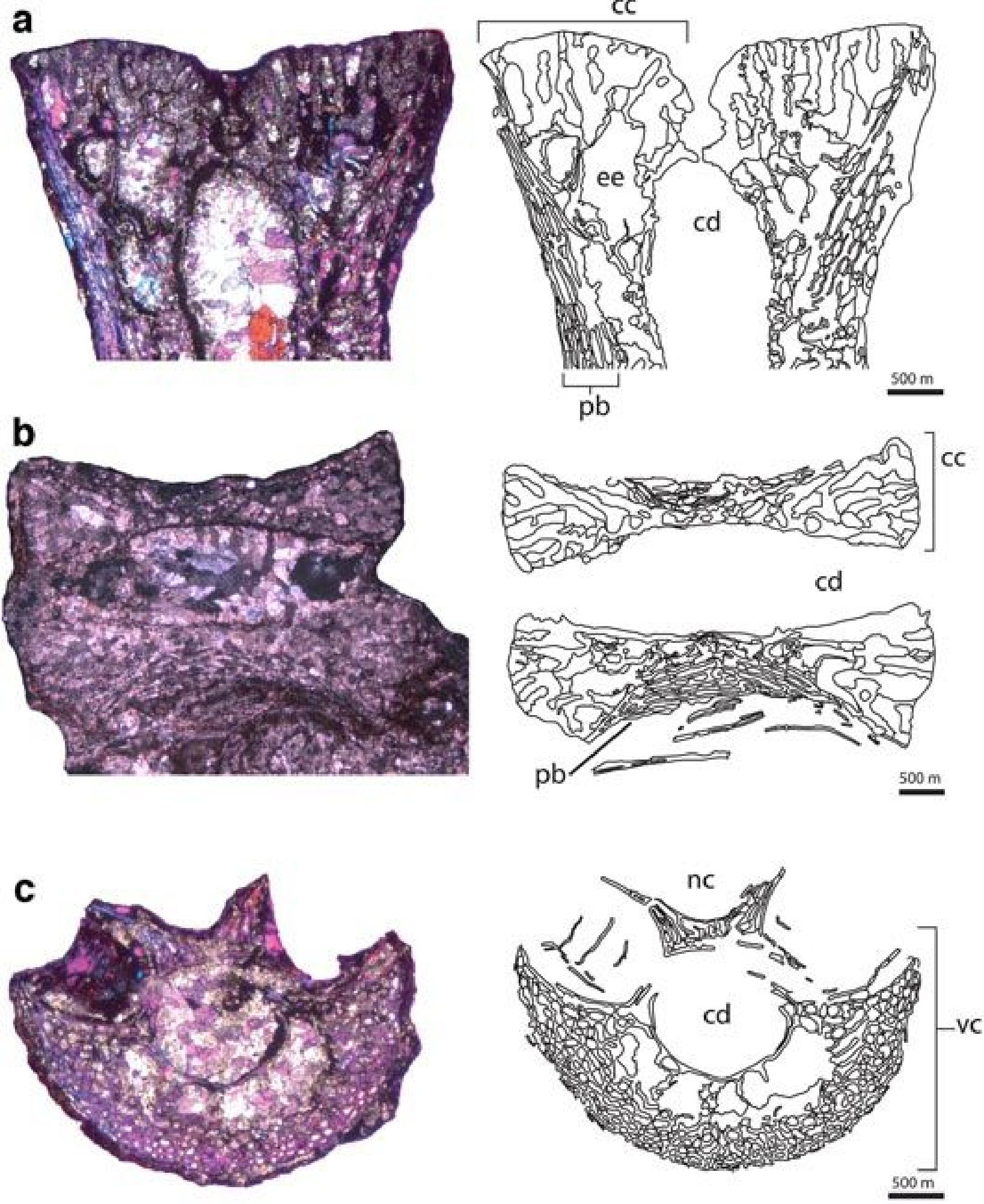
a
cc
ee
cd
pb
500 m
b
cc
cd
pb
500 m
c
nc
cd
vc
500 m

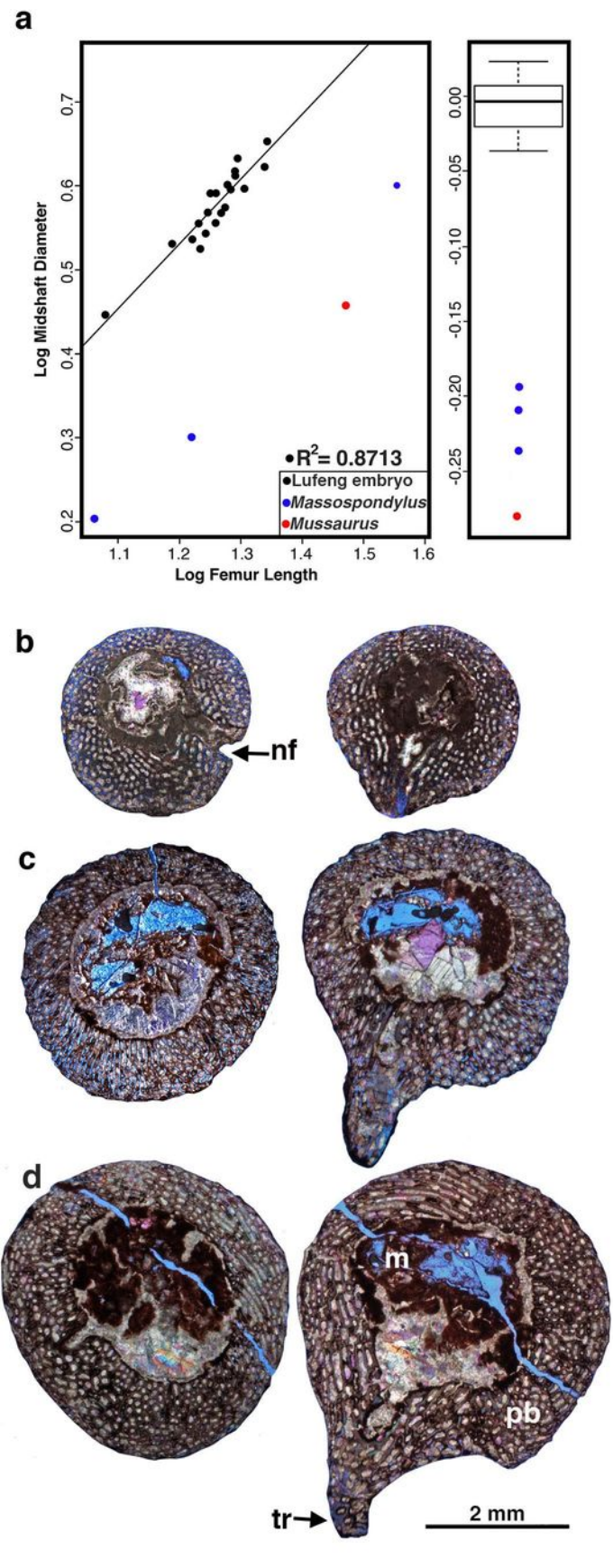
a
Log Midshaft Diameter
0.2
0.3
0.4
0.5
0.6
0.7
1.1
1.2
1.3
1.4
1.5
1.6
Log Femur Length
R^2= 0.8713
Lufeng embryo
Massospondylus
Mussaurus
0.00
-0.05
-0.10
-0.15
-0.20
-0.25
b
nf
c
d
m
pb
tr
2 mm

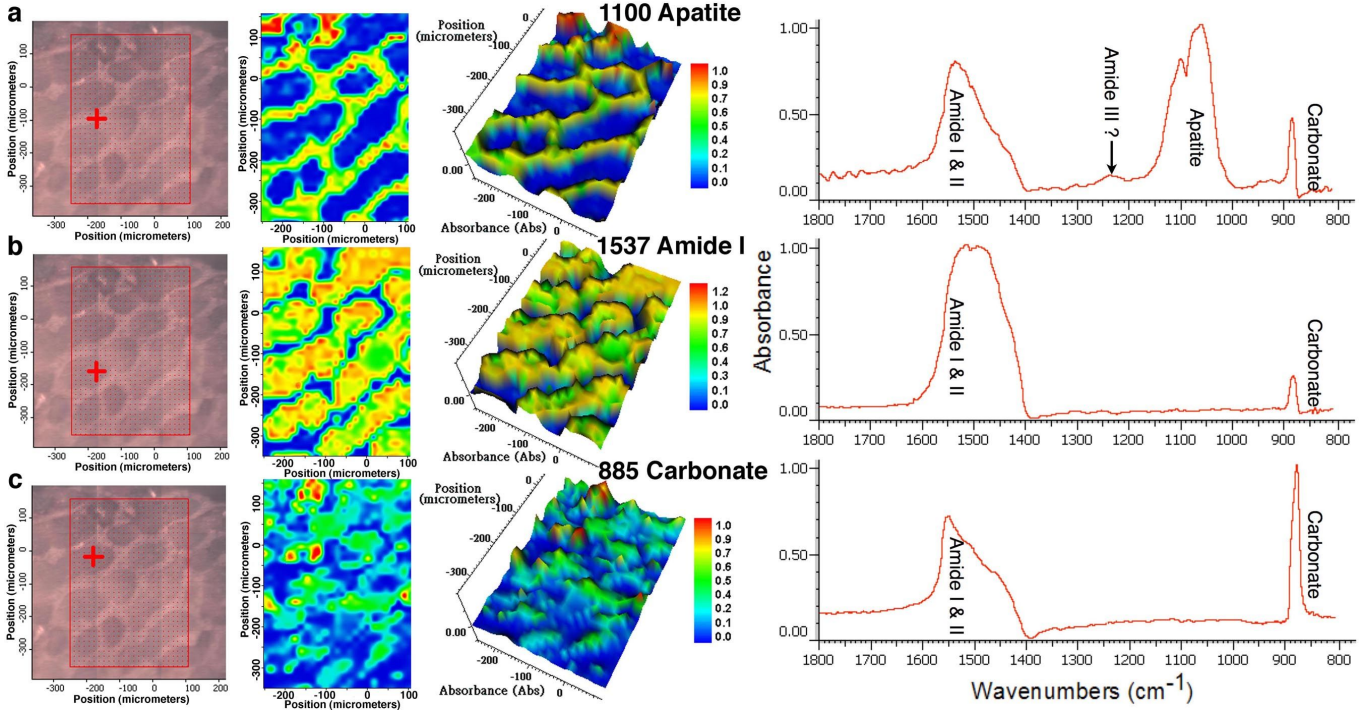
a
b
c
1100 Apatite
1537 Amide I
885 Carbonate
Position (micrometers)
Absorbance (Abs)
Absorbance
Amide I & II
Amide III ?
Apatite
Carbonate
Wavenumbers (cm-1)